NUMERICAL AND EXPERIMENTAL STUDY OF EROSION IN OPEN CHANNEL FLOW

Klemens Gruber[1], Christoph Kloss[1, 2] & Christoph Goniva[1, 2]

[1]Christian Doppler Laboratory on Particulate Flow Modelling, JKU Linz, Austria, Altenbergerstr. 69, 4040 Linz
[2]DCS Computing GmbH, Altenbergerstr 66 a, 4040 Linz, Austria
E-mail: klemens.g@gmx.net

Abstract

A new numerical model at particle-scale is proposed to simulate the erosion process in the presence of a free surface flow. The fluid flow is captured by a Computational Fluid Dynamics (CFD) method, where the sediment is modelled at a grain size level using Discrete Element Method (DEM). Its interaction is realized by a coupling of CFD and DEM. This Lagrangian approach allows capturing the physics of sediment erosion and deposition at a very detailed particle-scale level. The model is realized in an Open Source environment, based on OpenFOAM® and LIGGGHTS. Furthermore, the numerical simulations are tested against experimental work on sediment erosion downstream of a hydraulic structure. With the aid of optical and acoustic measurement techniques (PIV, ADV) the fluid flow is captured in the experiment, where bed deformation is captured by a LASER based measuring device. It is shown that the proposed numerical approach is suitable to correctly predict local erosion.

Introduction

Prediction of local sediment transport downstream of hydraulic structures is an important research field due to its significant practical value. Excessive local scour development can threaten the stability of hydraulic structures such as low and high head structures, weirs, spillways and culverts. Therefore an accurate prediction of scour depth and its evolution in time is crucial.

Scour problems have been extensively studied experimentally and numerically by many researchers in the past. Fist investigations on scour due to jet were done by Rouse (1939) and Eggenberger & Muller (1944). Additionally, Karim & Ali (2000) give a good overview of local scour studies performed in the past. Most recent investigations are based on low head structures (Karim & Ali (2000); Kumiawan et al. (2001); Liu & García (2008); Abdelaziz et al. (2010)).

In the present work, a 3D numerical model at particle-scale is presented and validated for the prediction of scour development. As river morphology is composed of complicated interactions of turbulent flow, the free water surface, particle motion and its resulting bed configurations, the fluid flow in the model is captured by a Computational Fluid Dynamics (CFD) method, which can deal with various turbulence models, where the water-air interface is captured by an Eulerian method, namely volume of fluid (VOF) method. The sediment is modelled at a grain size level using Discrete Element Method (DEM). Thus, particle-particle contact physics as well as fluid-particle forces are resolved in detail. To the author's knowledge, no other studies were performed for local scour problems with a similar approach.

First a general overview and the Governing Equations of the DEM and CFD method is presented. In addition, the coupling routine, momentum exchange as well as a brief discussion on the drag and lift force is given. In order to show the validity of the suggested model approach an open channel experiment with a hydraulic structure and erodible particle bed is designed and conducted. Numerical simulations are performed and thereafter the simulation results of fluid flow as well as scour are validated against the experimental data.

DEM Method

The Discrete Element Method was introduced by Cundall & Strack (1979). A very brief description of the method will be provided in this section. Further details on the contact physics and implementation issues are available in the literature (e.g. Poeschel & Schwager (2005); Zhu et al. (2007)).

The strength of the DEM lies in its ability to resolve the granular medium at the particle scale, thus allowing realistic contact force chains and giving rise to phenomena induced by particle geometry combined with relative particle motion, such as particle segregation by percolation. Thereby, the DEM is able to capture many different physical phenomena.

Thanks to advancing computational power, the DEM has become more and more accessible lately. On actual desktop computers, simulations of up to a million particles can be performed. On very large clusters, the trajectories of hundreds of millions of particles can be computed (e.g. Sandia (2009)).

Governing Equations

In the framework of the DEM, all particles in the computational domain are tracked in a Lagrangian way, explicitly solving each particle's trajectory, based on the force balances:

$$m_p \ddot{\boldsymbol{x}}_p = \boldsymbol{F}_{p,n} + \boldsymbol{F}_{p,t} + \boldsymbol{F}_{p,f} + \boldsymbol{F}_{p,b} + \boldsymbol{F}_{p,p} + \boldsymbol{F}_{p,v} \quad (1)$$

$$\mathbf{I}_p \frac{d\omega}{dt} = \mathbf{r}_c \times \mathbf{F}_{p,t} + \mathbf{T}_{p,r}\,, \quad (2)$$

where $\mathbf{F_{p,n}}$ is the normal particle-particle contact force, $\mathbf{F_{p,t}}$ is the tangential particle-particle contact force. $\mathbf{F_{p,p}}$ is the force caused by the pressure on the particle, which can be splitted into the force due to buoyancy and the pressure gradient force, of the piezometric pressure $p_{rgh} = p - \rho_f \mathbf{g}\cdot\mathbf{x}$. Where ρ_f denote the fluid density, $\mathbf{g}$ the gravitational acceleration and $\mathbf{x}$ the coordinate vector. $\mathbf{F_{p,v}}$ is the fluid viscous force acting on the grain.

$\mathbf{F_{p,f}}$ is the force that the fluid phase exerts on the particles, which will be described in further detail in section 2.3.3. Other body forces like gravity, electro-static or magnetic forces are summarized to $\mathbf{F_{p,b}}$.

Each physical particle is mathematically represented by a sphere with velocity $\mathbf{u_p}$, mass m_p and volume V_p. The translational and angular accelerations of a particle are based on the corresponding momentum balances. Using a soft-sphere approach, the particles are allowed to overlap slightly. The normal force tending to repulse the particles can then be deduced from this spatial overlap $\Delta\mathbf{x}_p$ and the normal relative velocity at the contact point, $\Delta\mathbf{u}_{p,n}$. The above mentioned forces and torques are summarized in Table 1. For further information the reader is referred to Kloss et al. (2010).

Table 1: Components of forces and torque acting on particle p.

Forces	Correlations
$\mathbf{F_{p,n}}$	$-k_n \Delta \boldsymbol{x_p} + c_n \Delta \boldsymbol{u_{p,n}}$
$\mathbf{F_{p,t}}$	$\min\left\{\left\lvert k_t \int_{t_{c,0}}^{t} \Delta \boldsymbol{u_p} dt + c_t \Delta \boldsymbol{u_{p,t}}\right\rvert, \mu_c \boldsymbol{F_{p,n}}\right\}$
$\mathbf{F_{p,b}}$	$\boldsymbol{g} m_p$
$\mathbf{T_{p,r}}$	$R_\mu k_n \Delta \boldsymbol{x_p} \frac{\boldsymbol{\omega_{rel}}}{\lvert\boldsymbol{\omega_{rel}}\rvert} \frac{d}{2}$
$\mathbf{F_{p,p}}$	$-\nabla(p) V_p = \left(\frac{1}{2}\rho_f \nabla \boldsymbol{u}_f^2\right) V_p + \rho_f \boldsymbol{g} V_p$
$\mathbf{F_{p,v}}$	$-\nabla \cdot (\boldsymbol{\tau}) V_p$
$\mathbf{F_{p,f}}$	$\mathbf{F}_D + \mathbf{F}_L$

LIGGGHTS is an open source software package for modelling granular material by means of the Discrete Element Method (LIGGGHTS, 2011). LIGGGHTS is a successful open source Molecular Dynamics code by Sandia National Laboratories for massively parallel computing on distributed memory machines (see Plimpton 1995). The code is designed to be easy to modify or extend with new functionality. Both LIGGGHTS and LAMMPS are distributed as open source codes under the terms of the GPL.

CFD-DEM Method

For the modelling of particle laden fluid flow a CFD-DEM approach can be applied (Tsuji et al. (1993); Zhu et al. (2007) (2008) and Zhou, Kuang, Chu & Yu (2010)).

The so called "non-resolved approach" presented here is applicable to those cases where particle sizes are smaller than the computational grid, thus the particles are assumed to not completely fill a computational cell.

Governing Equations

The governing equations modelling the behaviour of a free surface flow in the presence of particles can be interpreted as a synthesis of the Volume of Fluid (VOF) method, proposed by Hirt & Nicholls (1982), and the CFD-DEM method presented by Tsuji et al. (1993).

This approach results in a set of equations capturing the dynamics of three phases: the granular phase is captured by DEM, whereas the interstitial fluid composing of two phases (in our case water and air) is captured by the VOF method.

The equation of the fluid phase volume fraction α_1 can be written as

$$\frac{\partial \alpha_1}{\partial \mathrm{t}} + \nabla \cdot \left(\alpha_1 \alpha_f \boldsymbol{u_f}\right) - \nabla \cdot \left(\alpha_1 (1-\alpha_1) \boldsymbol{u_c}\right) = -\alpha_1 \frac{\partial \alpha_f}{\partial \mathrm{t}}, \quad (3)$$

where α_f is the volume fraction occupied by the fluid phases and $\mathbf{u_f}$ is the fluid velocity which can be replaced by the time averaged velocity for RANS / LES turbulence models.

In contrast to classical VOF method a source term at the right-hand side is introduced, which stands for the fluid displaced by particles. The third term on the left hand side is an artificial surface compression term with the compression velocity $\mathbf{u_c}$, which leads to a sharper interphase between the two different fluids (Rusche, 2002).

The motion of a fluid phase in the presence of a secondary particulate phase is governed by the volume-averaged Navier-Stokes-Equations for incompressible fluid. According to the idea of model type II (Zhou et al. (2010)), they can be written as:

$$\frac{\partial \left(\rho_f \alpha_f\right)}{\partial \mathrm{t}} + \nabla \cdot \left(\rho_f \alpha_f \boldsymbol{u_f}\right) = 0\,, \quad (4)$$

$$\frac{\partial \left(\rho_f \alpha_f \boldsymbol{u_f}\right)}{\partial \mathrm{t}} + \nabla \cdot \left(\rho_f \alpha_f \boldsymbol{u_f} \boldsymbol{u_f}\right) = \nabla \cdot \left(\alpha_f \boldsymbol{\tau}\right) - \alpha_f \nabla(p) + \alpha_f \rho_f \boldsymbol{g} + \sigma \kappa \frac{\boldsymbol{\nabla} \alpha_1}{\lvert\boldsymbol{\nabla} \alpha_1\rvert} - \boldsymbol{R_{pf}} \quad (5)$$

Here is ρ_f and μ_f are the fluid mixture density and viscosity, respectively, p the pressure and $\boldsymbol{\tau} = \mu_{eff}\left(\nabla \boldsymbol{u}_f + \left(\nabla \boldsymbol{u}_f\right)^T\right) - \frac{2}{3}\mu_{eff}\left(\nabla \boldsymbol{u}_f\right)\boldsymbol{I}$ is the stress tensor for the fluid phase, where the effective viscosity $\mu_{eff} = \mu_f + \mu_t$, is the sum of the mixture and the turbulent viscosity. α_f ρ_f **g** is the gravity force with the gravitational acceleration vector **g**, σ the surface tension and κ the curvature of the interface. $\mathbf{R_{pf}}$ represents the momentum exchange with the particulate phase, which is calculated for each cell, where it is assembled from the particle based drag and lift forces.

For solving above equations a pressure based solver using PISO pressure velocity coupling is used.

An overview of the CFD-DEM coupling routine is given in Goniva et al. (2011).

Fluid-Particle Momentum Exchange

Once the particle volume fraction is calculated it is possible to evaluate each particle's contribution to particle-fluid momentum exchange, which is established by means of a drag and lift force depending on the granular volume fraction.

For numerical reasons the momentum exchange term is split-up into an implicit and an explicit term using the cell-based ensemble averaged particle velocity $\langle \mathbf{u_p} \rangle$:

$$\mathbf{R}_{pf} = \mathbf{K}_{pf}\left(\boldsymbol{u_f} - \langle \boldsymbol{u_p} \rangle\right), \tag{6}$$

where $\boldsymbol{K}_{pf} = \frac{|\sum_i \boldsymbol{F}_{p,f}|}{V_{cell} \cdot |\boldsymbol{u_f} - \langle \boldsymbol{u_p} \rangle|}$.

Force models

For the calculation of the drag component of $\mathbf{K_{pf}}$ many different drag correlations have been proposed during the recent years (e.g. Zhu et al. (2007)).

Within this paper a drag relation based on lattice Boltzmann simulations recently proposed by Koch & Hill (2001) is used:

$$\overline{\boldsymbol{F}}_{\boldsymbol{D}} = \frac{V_p \beta}{\alpha_p}\left(\boldsymbol{u_f} - \boldsymbol{u_p}\right), \tag{7}$$

where β is a coefficient defined by Koch & Hill (2001), V_p is the particle volume and the particle volume fraction is defined by $\alpha_p = 1 - \alpha_f$.

So far, just the mean drag is considered, but for the initiation of sediment motion turbulent fluctuations and therefore the effective drag $\mathbf{F}_D = \overline{\mathbf{F}_D} + \mathbf{F}_D'$ is of importance (Zanke, 2003). Therefore, Zanke developed a model which considers the influence of velocity fluctuation. Based on $F_D = C_D \frac{1}{2}\rho A \boldsymbol{u}_r^2$ with $\mathbf{u_r} = \overline{\mathbf{u_r}} + \mathbf{u'_r}$, he proposed

$$\mathbf{F}_D = \left(1 + \frac{u'_r}{\overline{u_r}}\right)^2 \overline{\mathbf{F}_D}, \tag{8}$$

where $\overline{u_r} = |\mathbf{u_f} - \mathbf{u_p}|$ is the averaged velocity acting on the grain. By assuming Gauss distributed velocity fluctuations, u'_r can be expressed as $u'_r = n \cdot u'_{rms}$. Therefore, to model the turbulence, a Gauss distributed random number is used for n, as due to RANS Equation the direct turbulence information is lost. Hence (8) changes to $\mathbf{F}_D = \left(1 + \frac{n u'_{rms}}{\overline{u_r}}\right)^2 \overline{\mathbf{F}_D}$. Then the ratio $\frac{u'_{rms}}{\overline{u_r}} = f(k_s^+)$ at the bed can be expressed by the two known ratios u'_{rms}/u^* and $\overline{u_r}/u^*$ which are explained in the following.

Zanke gave an approximation for the universal velocity distribution law as a function of the distance of the grain at the bed surface to the wall $y=k_s$:

$$\frac{\overline{u_r}}{u^*}(y) = 0.8 + 0.9\left[\frac{1-P_t}{k_s^{+2}} + \frac{P_t}{\left(2.5\ln\left(\frac{y}{k_s}\right)+B\right)^2}\right]^{-0.5}, \tag{9}$$

where $B=(1-P_t)(2.5\ln(k_s^+ + 5.25)) + P_t 8.5$ and $P_t = 1 - e^{-0.08\ k_s^+}$. Furthermore, it is assumed that at the bed $y=d_p=k_s$ and therefore the non-dimensional roughness height k_s^+, is equal to the particle Reynolds number $Re_p^* = u^* d_p / \nu_f$. As now the only unknown is the friction velocity u^*, the universal velocity law can implicitly be solved with Newton's method.

Additionally, Zanke proposed a semi-empirical equation

$$\frac{u'_{rms}}{u^*} = 0.31 k_s^+ e^{-0.1 k_s^+} + 1.8 e^{-0.88 d_p/h}\left(1 - e^{-0.1 k_s^+}\right) \tag{10}$$

for rough walls (for $y=k_s$). Once again $k_s^+ = Re_p^*$ is assumed. The water level to grain diameter ratio h/d_p can be assumed as about 100. As u^* and therefore Re_p^* can be calculated implicitly due to the universal law of the wall, there are no more unknowns and equation (10) can be treated explicitly.

As the fluid volume fraction α_f is interpolated in the model and can therefore not represent the packed bed surface by a step in α_f, as a workaround the average drag $\overline{\mathbf{F}_D}$ at the bed surface is calculated with an α_f value of 0.5.

Beside the drag force resulting from a relative velocity between the particle and the fluid, the lift force is crucial for the initiation of sediment motion. The turbulent lift is the force due to turbulence induced pressure differences

between the upper and lower surfaces of the sediment grain. While dynamic lift has only a major significance for fully-exposed grains (Zanke, 2003), lift due to turbulence is the major lift component for packed grains.

Various different lift to drag ratios were measured and proposed by different authors. Chepil (1958) measured a constant ratio of about 0.85 for particle Reynolds number Re_p ranging between 47 and $5x10^3$ (Eqn. (12)).

Zanke was one of few who developed a theory of the influence of turbulence on the initiation of sediment motion. He proposed a lift to drag ratio at the bed

$$\frac{F_L}{|\boldsymbol{F_D}|} = \frac{1}{c}\left(\frac{u'_r}{u^*}\right)^2 \tag{11}$$

depending on the relationship of the velocity fluctuation acting on the grain to the friction velocity u^*. The constant c is given by Zanke with approximately 0.4. Furthermore, once again a Gauss distributed velocity fluctuation can be assumed and the ratio u'_{rms}/u^* can be express with Eqn. (10).

The direction of the turbulent lift force is perpendicular to the bed surface and thus given by $\mathbf{e} = \frac{\nabla \alpha_f}{|\nabla \alpha_f|}$. Summarized the turbulent lift force by "Chepil" and "Zanke", respectively is:

$$\boldsymbol{F}_{L,Chepil} = 0.85|\boldsymbol{F_D}|\boldsymbol{e}, \tag{12}$$

$$\boldsymbol{F}_{L,Zanke} = \frac{1}{c}\left(\frac{nu'_{rms}}{u^*}\right)^2 |\boldsymbol{F_D}|\boldsymbol{e}. \tag{13}$$

Other forces, caused by particle rotation (Magnus force), or particle acceleration (virtual mass force), are not applied in this study, but may be relevant for other problems. In the end the force of the fluid on the particle results in $\mathbf{F_{p,f}} = \mathbf{F_D}+\mathbf{F_L}$.

The modular implementation of the CFD-DEM coupling allows to easily implement additional forces and superpose all forces acting on a particle.

The method presented here treats the fluid and particle calculations in two strictly separated codes. This allows for taking advantage of independent code development on either side.

The interaction is realised by exchange fields being evaluated in a predefined time interval, where the codes work in a sequential manner. Both the CFD and the DEM code do their calculations in parallel using Message Passing Interface (MPI) parallelisation. Also data exchange between the codes is realised using MPI functionality.

The CFD-DEM approach described above was implemented within an open source environment (Goniva et al. 2011; Kloss et al. 2010). The DEM simulations are conducted by the DEM code LIGGGHTS (LIGGGHTS, 2011) and the CFD simulations are conducted by a solver realised within the open source framework of OpenFOAM® (OpenCFD Ltd., 2009). The coupling routines are collected in a library providing a modular framework for CFD-DEM coupling with the C++ codes LIGGGHTS and OpenFOAM®. Both, a selection of coupling routines as well as example solvers are provided at a dedicated web page maintained by the authors (CFDEM, 2011).

Experiment and Model Setup

Geometry and Experiment Setup

The experiments were conducted in an open channel test bench, without a slope (Figure 1). The flume is 4.12 m long and 0.4 m wide with a rectangular cross section. The experiment was carried out with and without an erodible bed, consisting of glass particles of 2 mm diameter. A weir is installed 0.9 m after the "Inlet Basin". The weir shape is a halved cylinder with a height of 95 mm.

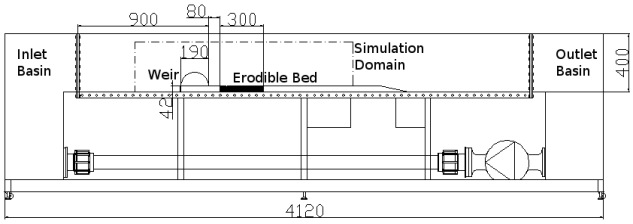

Figure 1: Schematic view of the test bench with the weir and an erodible bed. The pump is indicated at the bottom on the right and the particles of the erodible bed are indicated as circles. Additionally, the computational domain (dashed-dotted) is indicated in the schematic. (Length dimensions are in mm).

Water was pumped through the channel with constant flow rate. The water level upstream and downstream of the weir could establish freely, as no Spillway or control mechanism was used.

While the velocity field was observed with a PIV system, the erosion pattern was optically detected by using a LASER based device.

Boundary Conditions

The computational domain for the simulation is a sub-region of the open channel experiment (Figure 1). The inlet is 500 mm before and the outlet of the domain is 1000 mm behind the end of the weir. The height of the domain is 342 mm, whereby at the upper boundary ("Atmosphere") a symmetry boundary condition is applied. The mean velocity at the "Inlet" was observed by ADV

measurements, also the water level at the "Inlet" and "Outlet" are known from the experiment. Hence, these boundaries can be predefined within the simulation. At the "Outlet" boundary, the hydrostatic pressure boundary condition, $p_{rgh} = 0$ is applied (see also Table 2). For turbulent quantities wall functions are used. In order to save calculation time, a slice of 0.04 m width is considered, thus the resulting boundaries are treated as a symmetry.
The particle and fluid properties are listed in Table 3.

Table 2: Boundary Conditions

Boundary	**u** [m/s]	P [Pa]	h_w [m]
Inlet	(0.0285,0,0)	$\partial p/\partial \mathbf{n}=0$	0.157
Outlet	$\partial \mathbf{u}/\partial \mathbf{n}=0$	$p_{rgh}=0$	0.069
Walls	0	$\partial p/\partial \mathbf{n}=0$	$\partial \alpha_1/\partial \mathbf{n}=0$
Atmosphere	Symmetry	Symmetry	Symmetry

Table 3: Particle and fluid properties

Parameters	Value
Particle shape	Spherical
Particle diameter d_p [m]	0.002
Particle density ρ_p [kg/m^3]	2500
Rolling friction coefficient	0.01
Density of water ρ_w [kg/m^3]	998.2
Viscosity of water μ_w [kg/(ms)]	1 x 10^{-3}
Density of air ρ_a [kg/m^3]	1.2047
Viscosity of air μ_a [kg/(m s)]	1.78 x 10^{-5}
Surface tension σ [N/m]	0.07275

Results

Flow

In order to validate the numerical model, it is compared to the experimental measurements. In the following, first the simple flow over the weir without a particle bed is discussed, as sediment transport can be considered as a consequence of the flow. The most interesting result of the numerical and experimental investigation is the velocity profile. The velocity profiles are compared in the center plane of the channel. The numerical results are achieved with the k-ω SST turbulence model (Figure 2).

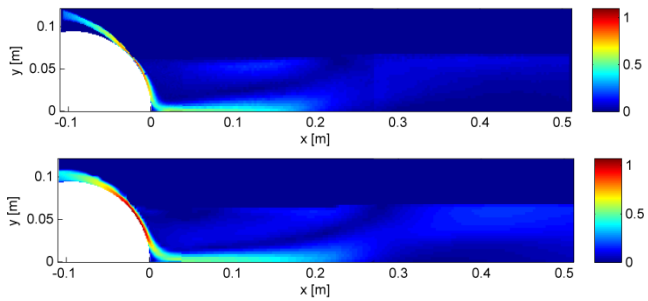

Figure 2: Comparison of the velocity [m/s] in the experiment (a) and simulation (b).

Furthermore, the velocity and its vector plot are compared in a restricted region (Figure 3), where sediment transport will take place in the case of an erodible bed.
Comparing the simulation with the experimental data, the highest velocity occurs downstream of the weir (Figure 2). Downstream the weir a submerged wall jet occurs at the bottom wall. Beneath the water surface a significant re-circulation region of the water develops, which provides more mass flux for the jet (Figure 3). Downstream this region the jet lifts.

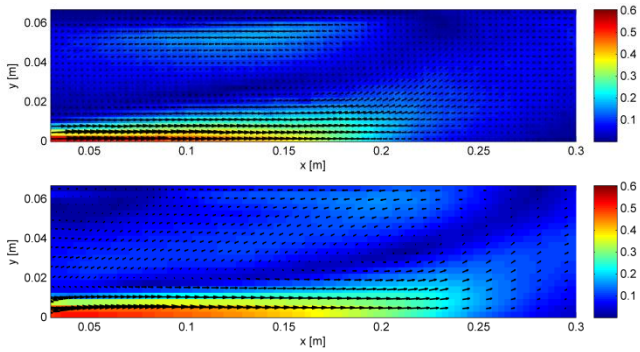

Figure 3: The velocity [m/s] and its vector plot in a restricted area are compared in the experiment (a) and simulation (b). The simulation show a further downstream rise of the jet and the recirculation direction differs slightly.

These phenomena are shown by the experimental investigations and are reproduced by the numerical simulation (Figure 3). Furthermore the velocity distribution compares well to the measurement data.

Erosion

So far the flow over a weir was compared with experimental data and a good match was shown. In the following section, the scour in an erodible erosion bed, resulting from the wall jet is discussed. The main interest lies in the comparison of different lift models and furthermore the temporal development of the scour will be investigated.
In the first step different turbulent lift models are applied, whereby the lift calculated with a fixed lift to drag ratio given by Chepil and the lift derived by Zanke, both discussed in the model section of this paper, are considered. The long term developed scour after 30 seconds underestimates maximum scour depth and height of the experimental data with the "Chepil" model, whereas "Zanke's" lift model gives better results, but also underestimates the data slightly (Figure 4). Furthermore, a simulation without a turbulent lift model is performed, which shows clearly less erosion.
Figure 5 shows the transient development of the scour. It can be seen, that onset of erosion takes place earlier within simulation than in experiment. Generally it is shown that the temporal scour formation of the simulation is in the

right time scale. The difference at the beginning may be due to a start with steady state flow for the simulation, while the experiment starts with an accelerating of the pump.

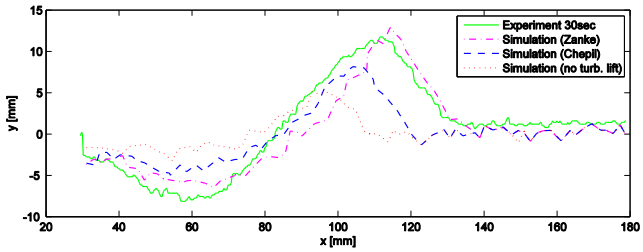

Figure 4: Comparison of the long term developed scour (30 sec) of numeric simulations with different lift models of "Zanke" (dashed-dotted), "Chepil" (dashed), without a turbulent lift model (dotted) and experimental measurement (solid line).

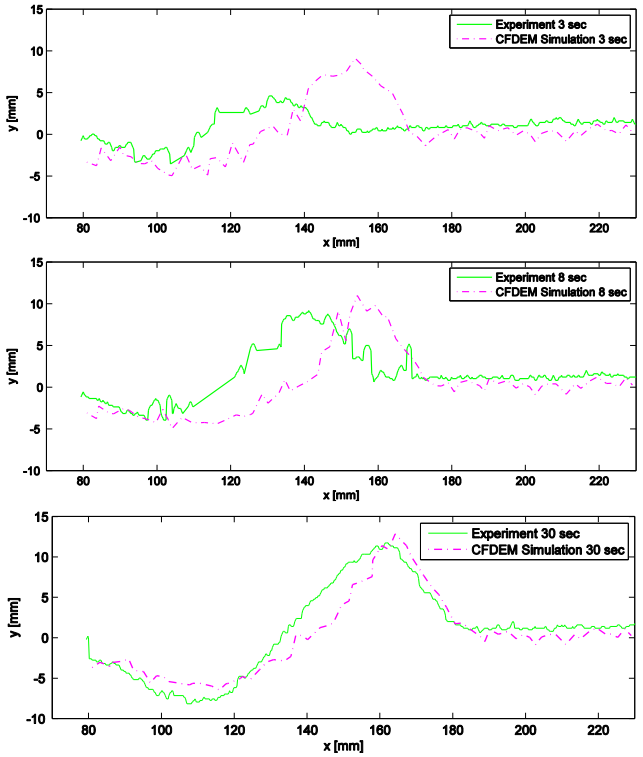

Figure 5: Comparison of the transient scour developed of simulation with the "Zanke" lift model (dashed-dotted) and experimental measurements (solid line).

Conclusion

A new numerical model was presented and validated for the prediction of scour development. It bases on a particle-scale approach with CFD-DEM, which can deal with a free surface. The model is realized in an Open Source environment, based on OpenFOAM® and LIGGGHTS. Thus, the model can easily be adapted to other applications and be further developed. An experiment of scour development after a hydraulic structure was conducted, where the validation of the model against the experimental data show excellent results for the proposed model. Additionally, it was shown that the turbulent lift force is essential for the initiation of sediment motion.

In the future the model should be validated for additional representative problems and also more applied conditions.

References

Abdelaziz, S., Bui, M. D., & Rutschmann, P. (2010). Numerical simulation of scour development due to submerged horizontal jet. *River Flow 2010. Proc. of the Intern. Conf. on Fluvial Hydraulics.*, (pp. 1597 – 1604). Braunschweig.

CFDEM. (2011). *CFDEM- Open Source CFD, DEM and CFD.* http://www.cfdem.com.

Chepil, W. (1958). The use of evenly spaced hemispheres to evaluate aerodynamic forces on soil surfaces. *Eos Trans. AGU*, pp. 397– 403.

Cundall, P., & Strack, O. (1979). A discrete numerical model for granular assemblies. *Geotechnique*, pp. 47-65.

Eggenberger, W., & Muller, R. (1944). "Experimentelle und theoretische Untersuchung über das Kolkproplem. *Mitteil., Versuchsanstalt f. Wasserbau. N0 5*.

Goniva, C., Kloss, C., Hager, A., Wierink, G., & Pirker, S. (2011). A Multi-Purpose CFD-DEM Approach. *8th International Conference on CFD in Oil & Gas, Metallurgical and Process Industries.* Trondheim Norway.

Hirt, C., & Nicholls, B. (1982). Volume of Fluid (VOF) Method for Dynamics of Free Boundaries. *Journal of Computational Physics*, pp. 201–225.

Karim, O., & Ali, K. (2000). Prediction of Flow Pat-terns in Local Scour Holes caused by Turbulent Water Jets. *J. of Hydr. Research, Vol.38*, pp. 279-287.

Kloss, C., Goniva, C., & Pirker, S. (2010). Open Source DEM and CFD-DEM with LIGGGHTS and OpenFOAM®. *Proc. Open Source CFD International Conference.* Munich.

Koch, D., & Hill, R. J. (2001). Inertial effects in suspension and porous-media flows. *Annual Review of Fluid Mechanics*, p. 619.

Kurniawan, A., Altinakar, M., & Graf, W. (2001). Flow Pattern of an Eroding Jet. *Proc. of XXIX IAHR Congress*, (pp. 537-544). Beijing, China.

LIGGGHTS. (2011). *LAMMPS Improved for General Granular and Granular Heat Transfer simulations.* http://www.liggghts.com.

Liu, X., & García, M. H. (2008). A 3D Numerical Model with Free Water Surface and Mesh Deformation for Local Sedi-ment Scour. *Journal of Waterway, Port, Coastal, and Ocean Engineering.*, pp. 203-217.

OpenCFD Ltd. (2009). *OpenFOAM - The open source CFD toolbox.* URL http://www.openfoam.com.

Plimpton, S. J. (1995). Fast Parallel Algorithms for Short-Range Molecular Dynamics. *J. Comp. Phys.*, pp. 1-19.

Poeschel, T., & Schwager, T. (2005). *Computational Granular Dynamics.* Springer.

Rouse, H. (1939). Criteria for similarity in the transportation of sediment. *Proc. Hyd. Conf. Studies Engineering Bull.*, pp. 33-39.

Rusche, H. (2002). *Computational Fluid Dynamics of Dis-persed Two-Phase Flows at High Phase Fractions.* London, UK.: Department of Mechanical Engineering, Imperial College of Science, Technology and Medicine. University of London.

Sandia. (2009). *LAMMPS User Manual.* http://lammps.sandia.gov/doc/Manual.html, Sandia National Laboratories, USA.

Tsuji, Y., Kawaguchi, T., & Tanaka, T. (1993). Discrete particle simulation of two-dimensional fluidized bed. *Powder Technology*, pp. 79-87.

Zanke, U. (2003). On the influence of turbulence on the initiation of sediment motion. *International Journal of Sediment Research*, pp. 17-31.

Zhou, Z. Y., Kuang, S. B., Chu, K. W., & Yu, A. B. (2010). Discrete particle simulation of particle-fluid flow: model formulations and their applicability. *Journal of Fluid Mechanics*, pp. 482-510.

Zhu, H., Zhou, Z., Yang, R., & Yu, A. (2007, July). Discrete particle simulation of particulate systems: Theoretical developments. *Chemical Engineering Science, 62, Issue 13,*, pp. 3378-3396.

Zhu, H., Zhou, Z., Yang, R., & Yu, A. (2008). Discrete particle simulation of particulate systems: A review of major applications and findings. *Chemical Engineering Science, 63*, pp. 5728-5770.